Hindawi
International Journal of Photoenergy
Volume 2022, Article ID 4401187, 19 pages
https://doi.org/10.1155/2022/4401187

Research Article

A Novel Topology to Improve PV Module Efficiency under Partial Shading Conditions

Dominique Bonkoungou,[1] **Toussaint Guingane**,[1] **Eric Korsaga**,[1] **Sosthène Tassembedo**,[1] **Zacharie Koalaga**,[1] **Arouna Darga**,[2] **and François Zougmore**[1]

[1]*Laboratory of Materials and Environment (LAME), University of Ouagadougou, P.O. Box 7021 Ouagadougou, Burkina Faso*
[2]*Group of Electrical Engineering, Paris (LGEP)11, Rue Joliot Curie, Plateau de Moulon, 91192 Gif sur Yvette, France*

Correspondence should be addressed to Dominique Bonkoungou; dominique.bonkoung@gmail.com

Received 13 September 2021; Revised 4 June 2022; Accepted 6 July 2022; Published 20 July 2022

Academic Editor: Mark Van Der Auweraer

In this paper, we investigate the power degradation in a novel photovoltaic (PV) cell reconfiguration named KenDoKu (KDK) topology under different shading patterns. We analyze how a modification in the linkage between the PV cells within a shaded PV module can affect its effectiveness. The proposed approach relocates the physical position of the PV cells within the PV module without any change in electrical connections and redistributes the shading effects over the PV module for the improvement of the power generation. To achieve this purpose, modeling and simulation are performed for a set of various shading patterns such as homogeneous, sectional, and scattered shadings. The simulation model used is a combination of two-diode model and Bishop's model. This model is applied to a PV module and is implemented in LTSpice software to quantify the impact of shading on P-V characteristics. The performance of the KDK topology is compared to other optimized configurations such as total-cross-tied (TCT), bridge link-total cross tied (BL-TCT), honey comb-bridge link (HC-BL), series parallel-total cross tied (SP-TCT) and existing odd-even (OE) and Latin square (LS) schemes of interconnection. The effectiveness of the KDK approach is evaluated in terms of the characteristics of P-V curves, global maximum power (GMP), mismatch power loss MPL (%), fill factor FF (%), and performance ratio PR (%). The simulated results revealed that the KDK configuration scheme performs better in terms of generating maximum power under the considered partial shading conditions. The proposed approach reduces the maximum power losses (MPL) and improves the fill factor (FF) with respect to OE and LS configurations in the most of the cases. Moreover, experimental verification is also carried out. The obtained results show that the KDK configuration outperforms the other analyzed PV cell rearrangement in terms of increased power.

1. Introduction

For the past three decades, PV technology has become attractive for renewable energy. The PV modules are widely used in urban as well as rural electrification. However, the PV module or system was far from satisfactory due to their low efficiency and high installation cost [1, 2]. The important current improvements have attracted the craze of researchers in the area of PV energy to deal with the problems presented in this field. Therefore, the enhancement of power is an open field of research, and therefore, the PV cell or module configuration technique is gaining more attention to address this problem [3].

The PV modules are often exposed to a number of factors that include wind, rain, heat, lightning, shading, and degradation effects over time, thus the performance of PV systems weather conditions dependent. In the literature, several studies have been carried out on the behavior of PV systems with various irradiances and temperatures to examine the change in solar irradiance and temperature effect on PV production systems [4]. The shading has predominant effect on the performance of PV modules, which thereby reduces significantly the generated power. Some PV cells or modules in the PV module/array receive various irradiance levels under partial shading conditions due to passing clouds, building, or trees, which may exhibit multiple local

peaks (LP) and one global peak (GP) on the output characteristics [4, 5]. The existence of multiple peaks may mislead the conventional maximum power point tracking technique by the local maximum power instead of global maximum power, which would add extra power loss to the PV module [1]. To extract the global maximum power, advanced MPP methodologies are employed [6, 7]. Due to an eventual malfunction of PV modules, a change in physical conditions or partial shading conditions may result in a low performance of PV modules [8]. To resolve these issues, Chao et al. [9] and Chen et al. [10] have proposed alternative approaches to minimize the power losses, whether dividing a PV array into a fixed and adaptive bank with an array switch or connecting bypass diodes across each cell. However, the addition of bypass diodes can exhibit multiple peaks in the output characteristics of the PV module [11]. To overcome these issues, a reconfiguration technique was used. The main goal of reconfiguration is to disperse the shading effects for uniform row current.

Belhachat and Larbes [12] have proposed a numerical approach based on the MATLAB program to analyze and compare various topologies of PV arrays for different shading patterns to find the best configurations that minimize power losses under partial shading conditions. However, they focused their work on a single situation of shading pattern.

To overcome partial shading issues, different configurations of PV cells/modules such as SP, BL, HC, TCT, BL-TCT, and hybrid SRBL-TCT are analyzed to achieve the desired output characteristics [13]. This work shows that the hybrid configurations have the best performance results compared to the other configurations.

Some studies have been conducted on the comparison between various solar panel topologies such as SP, HC, BL, and TCT. The results obtained show that, in general, the TCT configuration provides the best efficiency under different partial shading conditions [14, 15].

However, the TCT configuration has demerits, such as when the number of shaded PV cells are in the same row, that restricts the output characteristics of a PV module. To overcome this problem, Manna et al. [16] and Sai Krishna and Moger [17, 18] have developed reconfiguration methodologies for the TCT topology to dispatch shading effects from one row into various rows, in order to reduce the mismatch losses under partial shading conditions. Reconfiguration methodologies can be classified into two parts: dynamic and static techniques. Sai Krishna and Moger [17–19] have analyzed and discussed dynamic reconfiguration approaches. In these methodologies, PV modules are dynamically reconfigured within the PV array to enhance the output power generation under different partial shading conditions. However, the aforementioned research show that the dynamic reconfiguration approach necessitates the use of sensors to locate the shading, a complex algorithm to enhance the output power and a switching circuit. As a result, the dynamic reconfiguration is found to be complex and economically not feasible for a large PV system [20, 21]. Contrary to dynamic interconnection technique, the static methodology does not require any complex algorithms, sensors, and switching circuits. However, it requires an adequate design for organizing the location of PV cells to dispatch shading effects over the PV module. The authors [21–23] proposed novel interconnection schemes to eliminate partial shading effects over the PV array to enhance the PV power generation. However, all these proposed reconfigurations have one common demerit: they are not appropriate for PV arrays with unequal number of rows and columns. Therefore, to overcome these issues, the authors in [24] proposed zigzag reconfiguration scheme for TCT PV module configuration to enhance maximum power output under partial shading conditions. This reconfiguration technique alters the location of the PV modules in different columns. As a result, this complicates the interconnection scheme for a large PV module size. In ref [25], the authors introduced an improved permanent structuring technique named odd-even configuration to configure the PV module within the PV array in order to achieve maximum power output under partial shading conditions. The authors [26] presented a comprehensive and comparative study of the existing TCT configuration with a Latin square (LS) reconfiguration scheme to minimize shading effects. In this paper, the LS approach enables the reconfiguration scheme to redistribute shading effects over the PV array without altering the electrical connections. However, according to [25, 26], when PV modules are shaded across the entire rows, the PV array is reorganized into two (2) rows; this means that if the shade falls on the diagonal side of the PV array (see Figures 1(a) and 1(b)), it will stay undispersed. Consequently, this causes a decrease in maximum power generation. Furthermore, after the PV module rearrangement, when the shade occurs on the diagonal side, the shading effects are displaced in the first row. As a result, the output current is reduced. According to the literature review [27], it is obvious that static interconnection considered as one time arrangement is superior to electric reconfiguration. It does not dynamically alter the location of the PV module, since the PV module position is set for all shading conditions. However, the one-time interconnection technique is limited to use in a small PV system; this should be improved. To overcome these issues, this paper introduces a physical location alternative using Kendoku (KDK) arrangement for TCT PV module configuration. The KDK technique redistributes the shading effect over the PV cells in a PV module, and therefore, mismatch losses are reduced. The proposed KDK arrangement approach minimalizes the number of shaded PV cells in a single row significantly and can be applied to PV module of any size. The effectiveness of the KDK arrangement is evaluated by analyzing the P-V characteristics under partial shading with other optimized arrangements techniques such as:

(i) Total cross-tied (TCT) configuration as shown in Figure 2(a)

(ii) Bridge-link total cross-tied (BL-TCT) configuration: it has the same number of components of TCT topology, but with an interconnection wiring as shown in Figure 2(b)

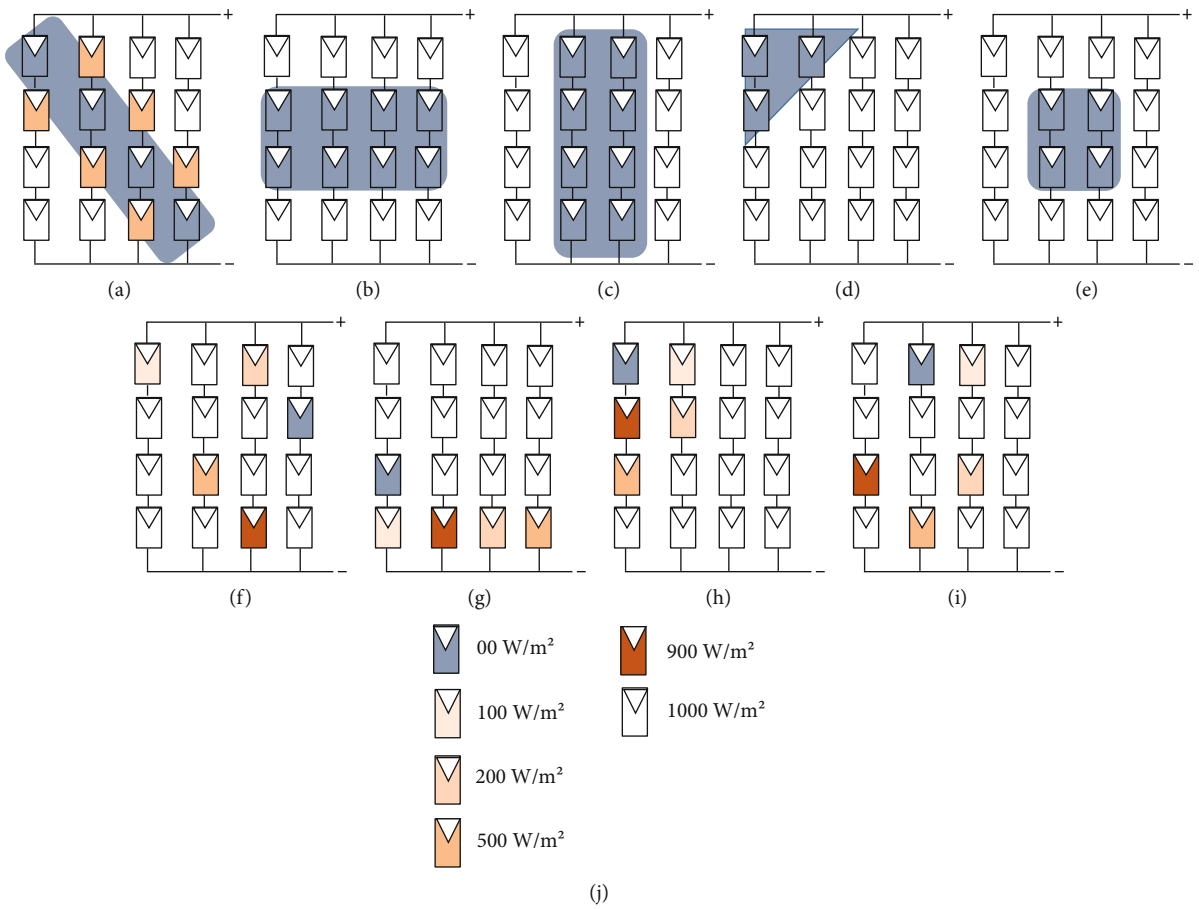

Figure 1: Definition of different shading models under partial shading conditions: (a) DS pattern, (b) FS pattern, (c) VS pattern, (d) CS pattern, (e) CLS pattern, (f) SS-pattern A model, (g) SS-pattern B model, (h) SS-pattern C model, (i) SS-pattern D model, and (j) degree of irradiation levels on PV cells.

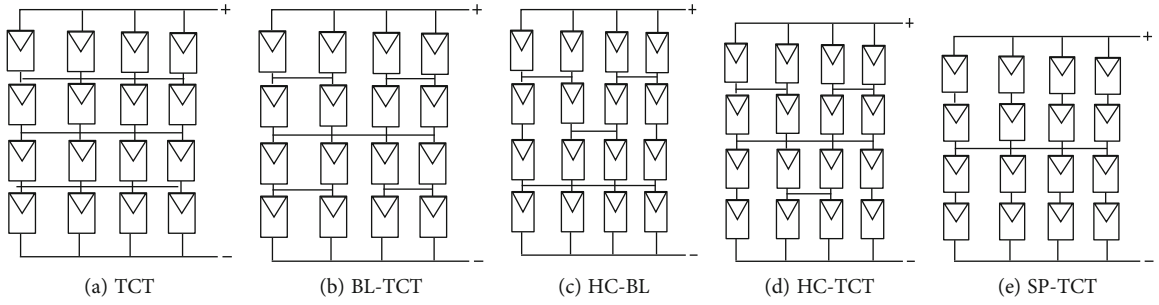

Figure 2: PV module topologies used for comparison.

(iii) Honey comb-bridge link (HC-BL) configuration combines HC and BL topologies shown in Figure 2(c)

(iv) Honey comb total cross-tied (HC-TCT) combines HC and TCT configurations shown in Figure 2(d)

(v) Series parallel-total cross-tied (SP-TCT) is also a combination of SP and TCT configurations presented in Figure 2(e)

Moreover, an extensive analysis on existing odd-even (OE) [25], Latin square (LS) [26] reconfigurations, and KDK is carried out to verify the applicability of the proposed technique by comparing the GMP, ML (%), FF (%), and PR (%) under different shading conditions.

2. Mathematical Modeling

2.1. Modeling of PV Cells. Generally, a classical one diode or two diodes is used as an equivalent circuit of PV cells. The advanced two-diode model is widely used as it better matches the experimental curves of PV cells. For PV cells, which are driven in the negative voltage range, the model has the ability to describe the breakdown region at high

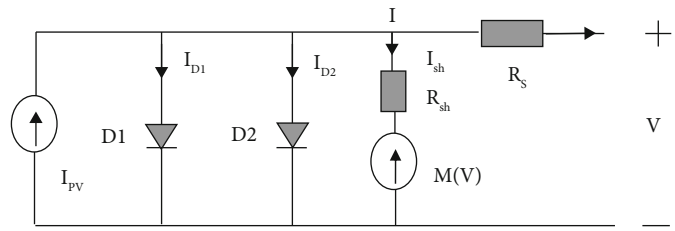

Figure 3: Solar cell equivalent circuit.

negative voltages. This is essential to be taken into account in the study of PV cells working partially shaded, forming part of a PV module. In this case, Bishop [28] proposed an equation in which the avalanche effect is expressed as a nonlinear multiplication factor that affects the shunt resistance current term, using the simple diode model. In the present work, we use a combination of the two-diode model and Bishop's model, to study the electrical behavior of solar cells working partially shaded. Figure 3 shows the PV cell equivalent circuit considering the avalanche effect.

Kirchhoff's first law carries the following relationship between PV cell current and voltage:

$$0 = f(V, I) = I_{PV} - I_{D1} - I_{D2} - I_{sh} - I. \tag{1}$$

Then, the photon-generated current can be calculated using Equation (2), which describes the I-V characteristics of a partially shaded PV cell considering the avalanche breakdown voltage.

$$\begin{aligned} I = {} & I_{PV} - I_{01}\left[\exp\left\{\frac{(V + R_S I)}{a_1 V_T}\right\} - 1\right] \\ & - I_{02}\left[\exp\left\{\frac{(V + R_S I)}{a_2 V_T}\right\} - 1\right] - \frac{V + R_S I}{R_{Sh}} \\ & - a\left(\frac{V + R_S I}{R_{Sh}}\right)\left(1 - \frac{V + R_S I}{V_{br}}\right)^{-m}, \end{aligned} \tag{2}$$

where $V_T = kT/q$ is the thermal voltage, I_{PV} is the current generated by the incident light, q is the electron charge, k is the Boltzmann constant, T is the temperature of the $p-n$ junction, R_S is the series resistance, and R_{Sh} is the shunt resistance. I_{01} and I_{02} are the reverse saturation currents of diode 1 and diode 2, respectively. The extension term $M(V)$ is added to the leakage current in the shunt resistance term modeled as a controlled current source:

$$M(v) = a\left(\frac{V + R_S I}{R_{Sh}}\right)\left(1 - \frac{V + R_S I}{V_{br}}\right)^{-m}, \tag{3}$$

where V_{br} is the avalanche breakdown voltage, m is the avalanche breakdown exponent ($1 \le m \le 10$), and a the correction factor.

2.2. Modeling of the PV Module. A PV module is a combination of PV cells in series or parallel to enhance the required electrical power. In the case of series connected PV cells, the I-V characteristic is derived by adding the induced voltages at the same output current, whereas, in the case of parallel connected PV cells, the induced currents will be added at the same terminal voltage [29]. Theoretically, the parameters to be added will be a multiple of one parameter and the number of cells assuming identical PV cells. The experience has shown that this assumption is not always valid. Although the PV cells are characterized with the same specifications, there are slight differences during the manufacturing points under the same insolation level. This phenomenon is known as mismatched operation of PV cells. Thus, the model described in Section 2.1 for a PV cell can be extended to a PV module consisting of Ns series PV cells and Np parallel PV cells [29]. The numerical equation for the current I of a PV module arranged in N_P parallel and N_S series PV cells becomes:

$$\begin{aligned} I = {} & N_P I_{PV} - N_P I_{01}\left[\exp\left\{\frac{q(V + \gamma R_S I)}{N_S . a_1 V_T}\right\} - 1\right] \\ & - N_P I_{02}\left[\exp\left\{\frac{q(V + \gamma R_S I)}{N_S a_2 V_T}\right\} - 1\right] \\ & - \left(\frac{V + \gamma R_S I}{\gamma R_{Sh}}\right) - (G(V)), \end{aligned} \tag{4}$$

where $\gamma = N_S/N_P$; $G(V)$ is given as follows:

$$G(V) = a\left(\frac{V + \gamma R_S I}{\gamma R_{Sh}}\right)\left(1 - \frac{V + \gamma R_S I}{V_{br}}\right)^{-m}. \tag{5}$$

3. Experimental Setup

3.1. Procedure for Parameter Extraction. The PV cell model used in this research work is based on the model presented in the reference [13]. The proposed topology KDK consists of n parallel strings; each string contains n series components. Each component is protected by antiparallel bypass diode. Basically, we assume that all PV cells in the PV module are homogeneous, and there is no mismatch between them. We used, for the simulation, LTSpice software to implement the relationships described in the previous Equation (4). LTSpice is a high-performance simulation program with integrated circuit emphasis (SPICE) simulator. Different scenarios are simulated for various PV cell sizes. The current-voltage (I-V) curve for each component cell in the PV module is characterized by PV cell specific parameters' values. The parameters of a typical solar cell named KX0B22-12X1F are used for our modeling and simulation [30]. It is a complementary study of a previous work in which the parameters of the PV cell extracted under dark/

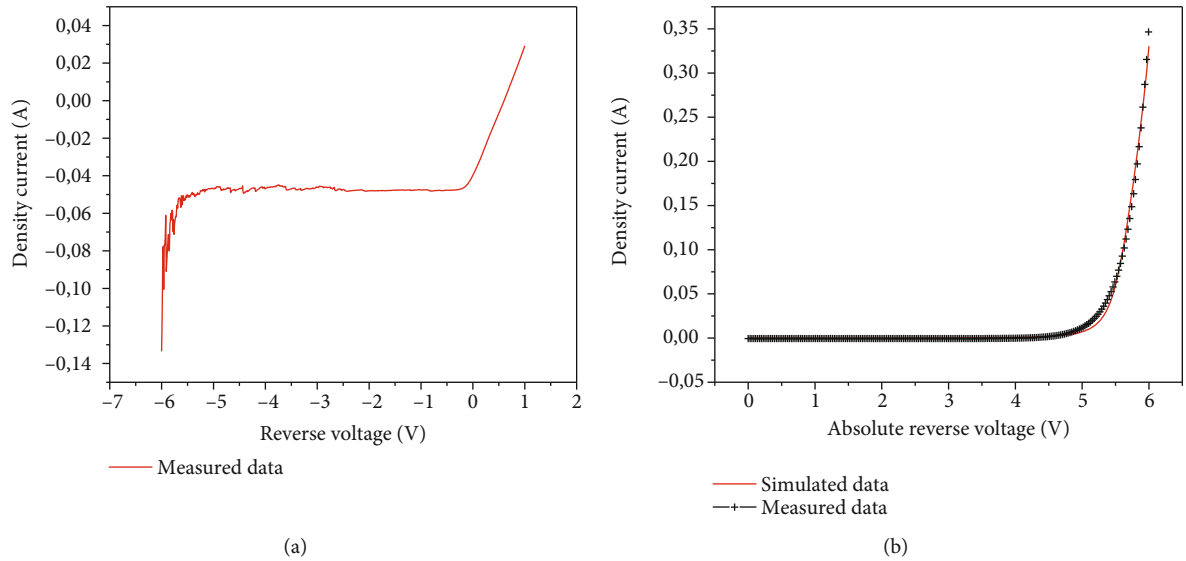

Figure 4: Comparison between the I-V characteristics of a PV cell in receiver mode: measured data versus simulated data.

Table 1: Extracted parameters used in the simulation model.

Parameters	Values
$I_{01}(\mathrm{A/cm^2})$	3,126 10^{-13}
$I_{02}(\mathrm{A/cm^2})$	2,798 10^{-7}
a_1	1.035
a_2	2.34
$R_S(\Omega * \mathrm{cm^2})$	6.24
$R_{Sh}(\Omega * \mathrm{cm^2})$	134 184
a	0.256
V_{br}	-5.96
m	3
$T(^{\circ}\mathrm{K})$	300

light conditions by using a nonlinear least squares method [30, 31]. For Bishop Parameter's extraction, a fit of the I-V characteristic is carried out under dark condition by using the measurement data as shown in Figure 4. The data are measured in forward and reverse direction. The values of the extracted parameters are presented in Table 1.

The photocurrent source is influenced by four parameters, such as irradiation, temperature, the area of the PV cell, and short circuit current. For this study, the PV cell used has an area of 270 $\mathrm{mm^2}$ and a short circuit current density of 42, 4 $\mathrm{mA/cm^2}$.

3.2. Shading Patterns Used in the Simulation. The shading models used for the experiment are presented and categorized into three parts.

(i) Homogeneous shading: in this shading pattern, all considered PV cells receive the same shading rate. Based on the number of shaded PV cells per column (string) and the number of shaded columns, we define three shading conditions as shown in Figures 1(a)–1(c)

(a) Diagonal shading (DS) pattern

(b) Flat shading (FS) pattern

(c) Vertical shading (VS) pattern

(ii) Sectional shading: contrary to homogeneous shading, in sectional shading, the considered PV cells receive different rates of shading or irradiation. In this study, two types are considered as presented in Figures 1(d) and 1(e)

(a) Corner shading (CS) pattern

(b) Central localized shading (CLS) pattern

(iii) Scattered shading (SS) pattern: in this shading condition, we defined four shading patterns named as SS-pattern A, SS-pattern B, SS-pattern C, and SS-pattern D as illustrated in Figures 1(f)–1(i)

Besides, the defined solar irradiance levels or shading rates of each PV cell are described in Figure 1(j), in which 1000 $\mathrm{W/m^2}$ means that there are not shaded PV cells in the module. On the other hand, 500 $\mathrm{W/m^2}$ means that 50% of the area of the PV cells is covered by shade.

4. Results and Discussion

4.1. Modeling and Simulation of PV Module under Shading Conditions. As defined previously, the model of Bishop is adopted in this research paper to analyze PV modules operating in uniform, partial or full shading conditions. Figure 5 presents the output characteristics (current-voltage (I-V) and puissance-voltage (P-V)) of an example of PV module topology operating in normal (uniform) and abnormal or partial shading conditions. In normal conditions,

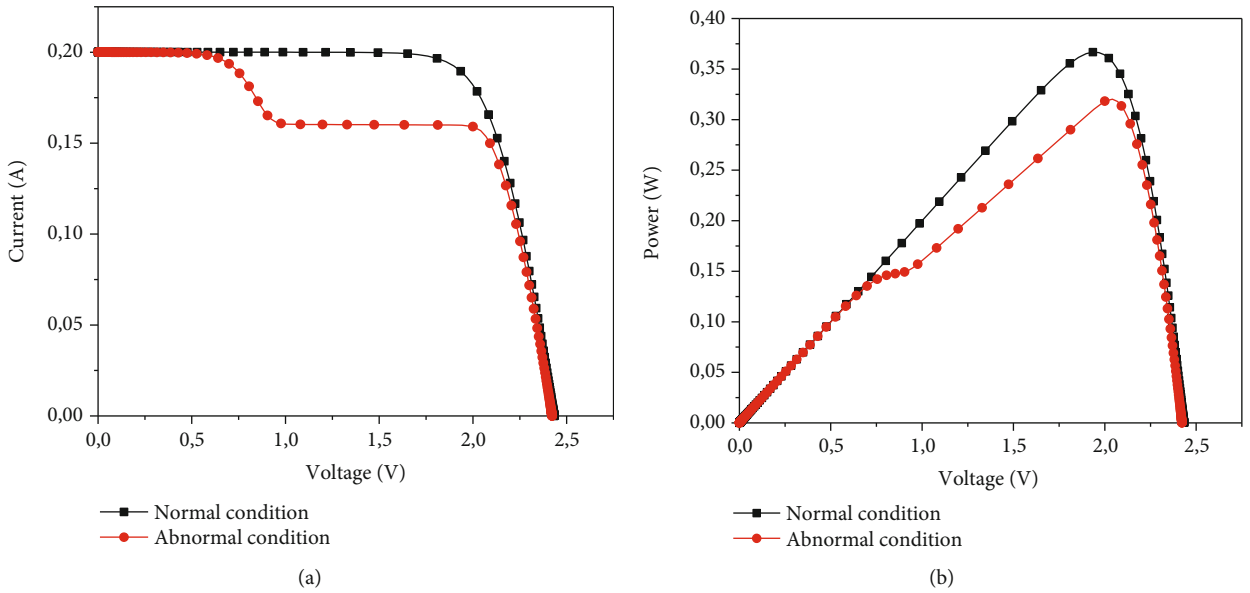

Figure 5: Output characteristics of PV module operating in normal and partial shading conditions: (a) *I-V* characteristics and (b) P-V characteristics.

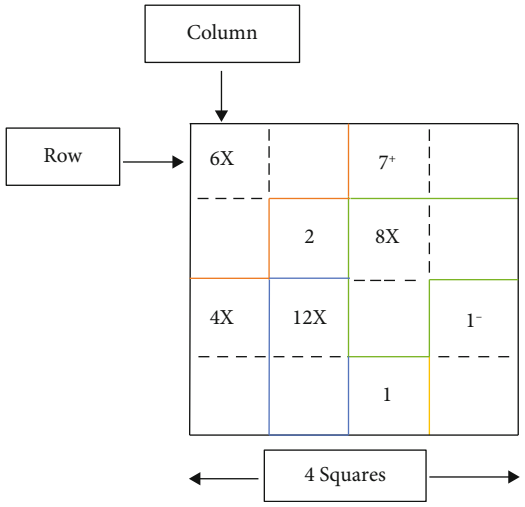

Figure 6: An example of a 4×4 rebus pattern with 8 cages considered for this study.

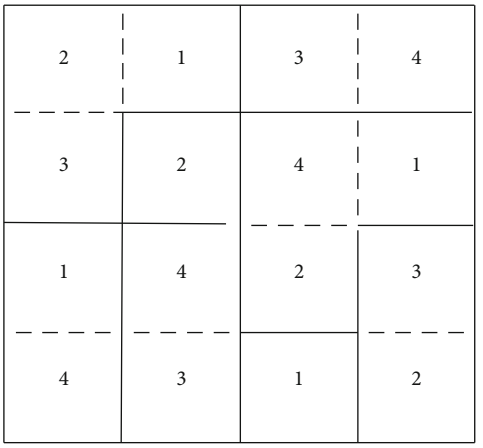

Figure 7: Basic solution of the proposed 4×4 KDK rebus pattern.

temperature and irradiance are defined in the standard test condition (STC) (at 25°C and 1000 W/m^2) while in abnormal conditions, various levels of irradiance are defined: two PV cells are exposed to 500 W/m^2 and 700 W/m^2, respectively.

As seen in Figure 5, the shading increase in the rate of the cell produces a higher reduction of short circuit current I_{SC}, which causes a reduction in the maximum power. It clearly demonstrates that the cell-generated current is a function of the rate of light transmittance. Under normal conditions, the maximum power of a PV module is 0.37 W at a maximum voltage equal to 1.93 V. When shading occurs, a considerable reduction of the power is observed. The P-V curve also presents two local maximum peaks. The first maxima localized very far from the normal maximum power point (at $P = 0.80$ W and $V_{oc} = 0.14$ V) zone is independent of the irradiance or shaded PV cell area, as the number of shaded PV cells is short-circuited. On the other hand, the second maxima is the function of the number of shaded PV cells and their irradiance.

4.2. Proposed KDK Topology. Our method used a rebus to a power production. KDK is a rebus which requires the use of the digits to supplement a collection of cells named cages. It involves $n \times n$ or $m \times n$ grid which is divided into irregular cages. In each cage, a number and an arithmetic operation are affected as shown in Figure 6.

The principle is described as follows:

(i) Each square cell in the grid will contain a digit between 1 and the size of the grid. For the 4×4 grid, we use the digits 1, 2, 3, and 4

11	12	13	14
21	22	23	24
31	32	33	34
41	42	43	44

(a)

21	12	33	44
31	22	43	14
11	42	23	34
41	32	13	24

(b)

Figure 8: PV cell interconnections: (a) TCT and (b) KDK arrangement.

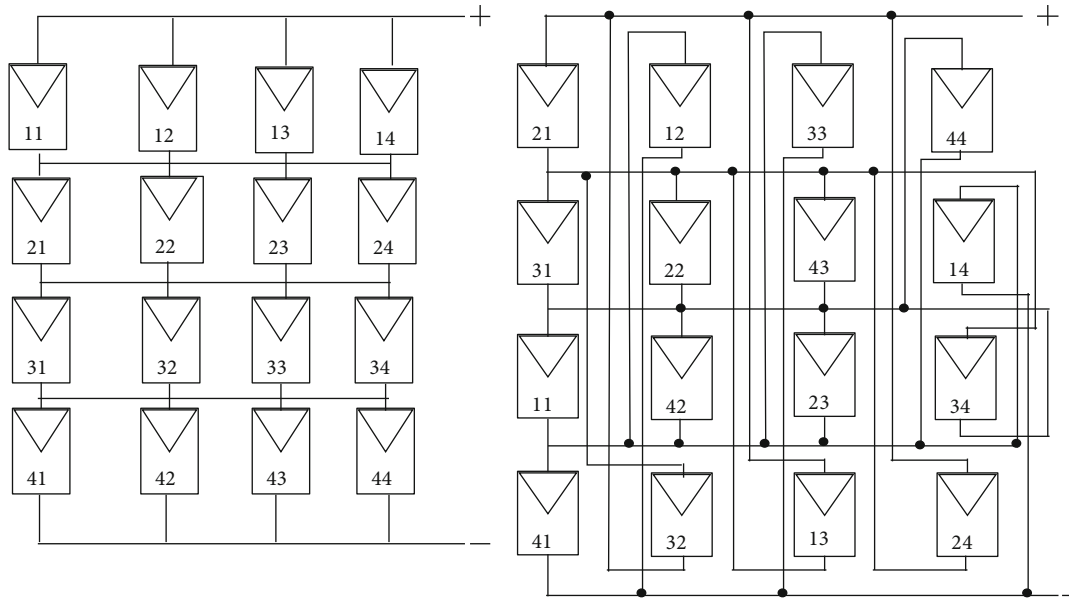

(a) TCT topology (b) Proposed KDK topology

Figure 9: Electrical interconnections of the PV cells in a PV module.

(ii) Each of the digits 1 to 4 must appear in each row and each column

(iii) No digit can repeat within any row or column

4.2.1. Solution Strategies. As mentioned previously, the solution requires that a 4×4 puzzle contains the numbers 1 through 4 exactly once in each row and column in any order. Whether there is no arithmetic operation denoted in a 1×1 cage, this digit is to be inserted into the cage. The operations such as sum or product of the digits in a cage have to yield the goal digit when the operation is (+) or ($\times$). On the other hand, when the operation is (−) or ($\div$), the cage must consist to two squares, and the difference or quotient of the two digits must yield the goal digit. The complete solution of 4 $\times$ 4 KDK rebus is presented in Figure 7.

4.2.2. Proposed KDK Arrangement. The considered PV module consists of 16 cells with 4 rows and 4 columns. In the traditional system of interconnection, the PV cells (forming a PV module) or modules (forming a PV array) are settled as in Figure 8(a). The puzzle settlement of the KDK topology is presented in Figure 8(b), in which the first number in each lodge indicates the row number and the second digit refers to the column number of the 4×4 PV module.

The electrical nexus of PV cells for the TCT topology is shown in Figure 9(a). According to the KDK pattern, the reconfiguration of TCT topology is presented in Figure 9(b).

4.3. Simulation and Analysis of the Proposed Topology of the PV Module Operating in Partial Shading Conditions. In this section, we evaluate the P-V output characteristics for various topologies operating in partial shading conditions. As

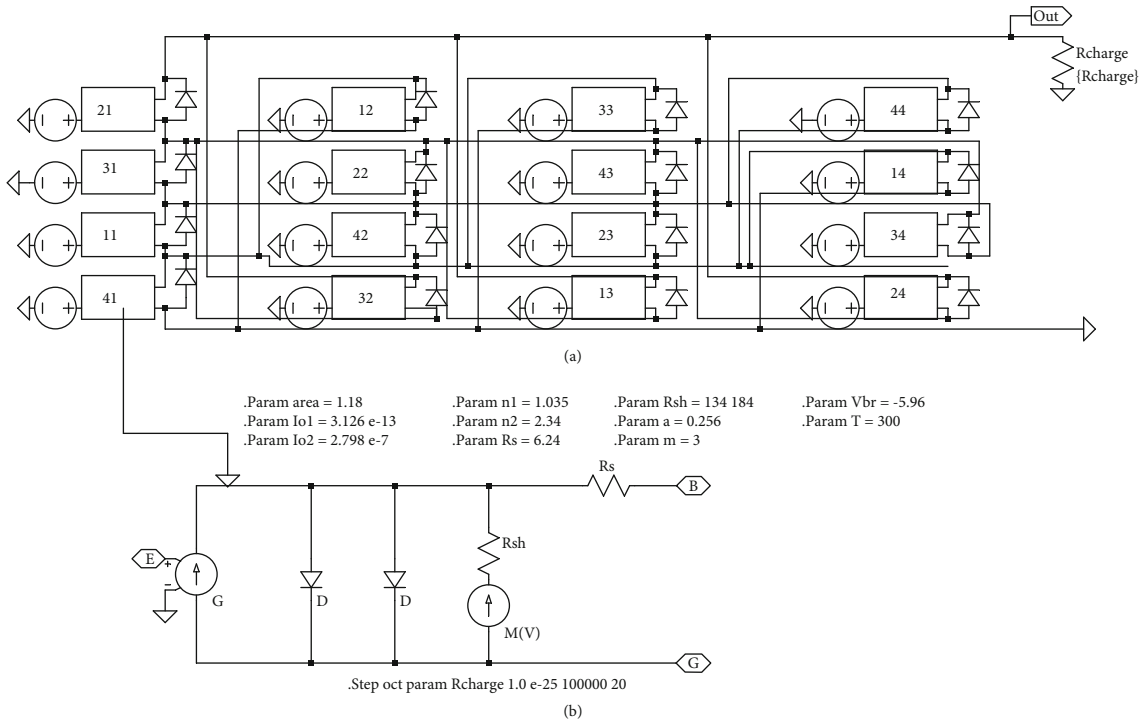

Figure 10: Circuit of the PV module used in LTSpice software: (a) PV module model and (b) PV cell model.

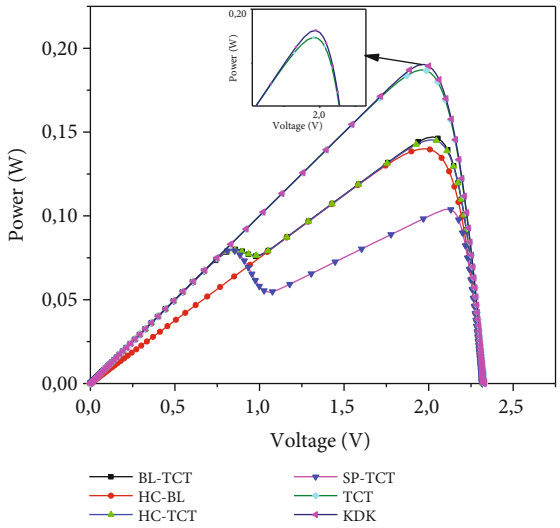

Figure 11: P-V characteristics of various PV module topologies operating in diagonal shading condition.

mentioned previously, a 4×4 PV cells is used for simulation and analysis. Thus, we performed our experiments for the simulation test with homogeneous and heterogeneous impacts on light *I-V* curves. We compared the proposed KDK topology with traditional topologies such as TCT, BL-TCT, HC-BL, HC-TCT, and SP-TCT. Their efficiencies are analyzed on the P-V characteristics for different solar irradiance levels, as presented in Section 3. The electrical LTSpice model of the PV cell and the circuit arrangement of KDK topology of the PV module used for the simulation are presented in Figure 10.

Case 1. Homogeneous shading conditions.

Figure 11 shows the P-V characteristics obtained by simulating the different topologies under the DS condition. We can see that most of the topologies exhibit some maxima on the P-V characteristics. Among all topologies, KDK topology generates a better profile. We can see from the P-V curves presented in Figure 12(a) that the rate of power degradation is much higher when the shading is flat for all topologies except the KDK topology, which shows a better performance in homogeneous shading conditions. However, in VS condition as shown in Figure 12(b), all topologies demonstrate a similar profile that generates the same maximum power point.

Case 2. Sectional shading pattern condition.

From Figures 13(a) and 13(b), it can clearly see that KDK topology is still better under sectional shading conditions, particularly in CS condition. Meanwhile, the HC-BL and SP-TCT topologies provide the lowest efficiency, in CS-pattern and CLS-pattern, respectively. Indeed, the more number of series connections in a string involves some mismatching losses under CLS-pattern condition.

Case 3. Scattered shading (SS) pattern condition.

Figure 14 shows the P-V characteristics of various PV module typologies operating in SS-pattern condition. The results show that KDK topology is greater in terms of maximum output power compared to other topologies under different shading patterns such as SS-pattern A, SS-pattern B, SS-pattern C, and SS-pattern D. KDK topology provides the best efficiency with low power dissipation compared to the others. From the obtained results, it is seen that the

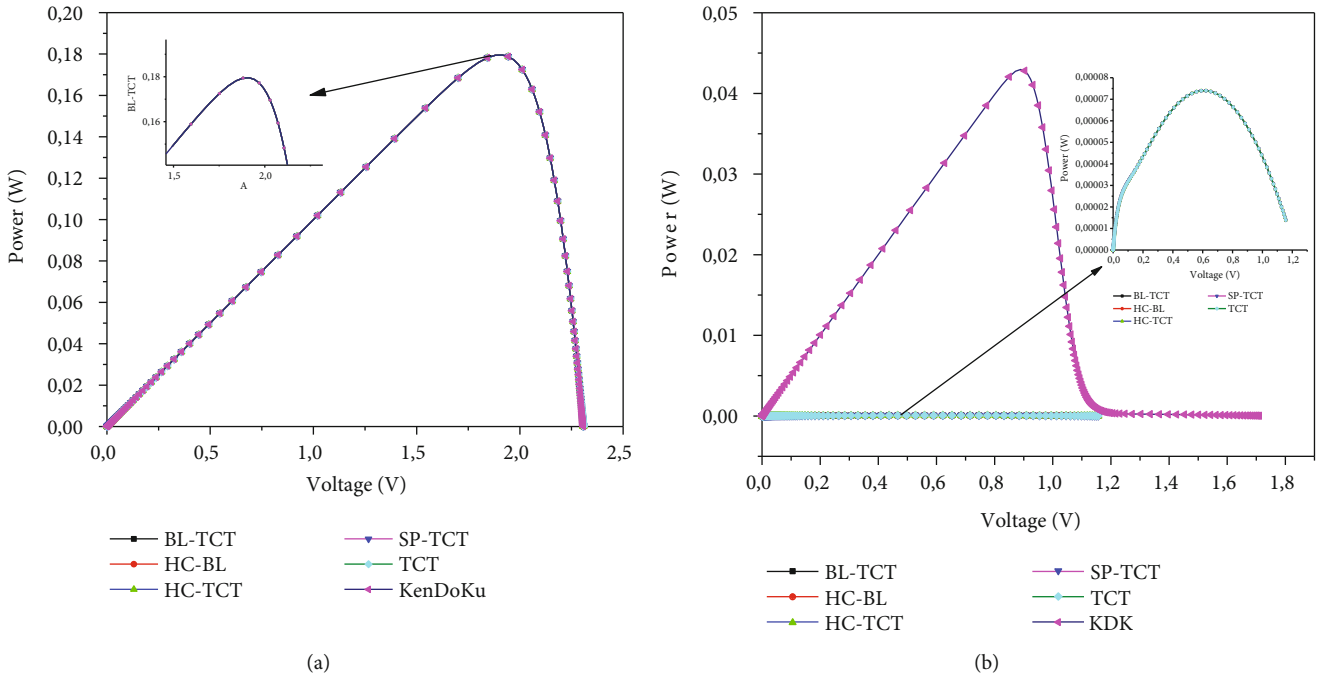

Figure 12: P-V characteristics of various PV module topologies operating in (a) FS-pattern and (b) VS-pattern.

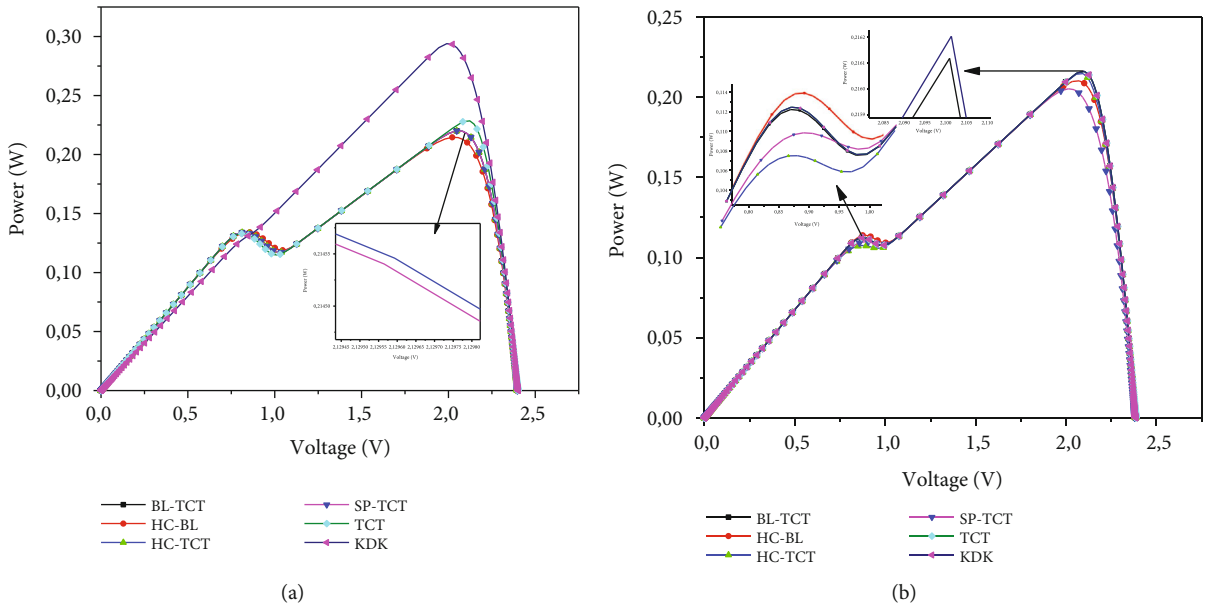

Figure 13: P-V characteristics of various PV module topologies operating in (a) CS-pattern and (b) CLS-pattern.

HC-BL topology (in Figure 14(c)) and SP-TCT topology (in Figures 14(a), 14(b), and 14(d)) are less interesting no matter the shading pattern. Among all the configurations, KDK topology is seen to be the most adequate in providing the optimal power by attenuating the power losses under SS-pattern condition.

4.4. Performance Evaluation. To select the best PV module topology which provides the highest efficiency, we compare the various topologies in terms of power loss percentage ($\Delta\theta_{\text{Loss}}$) operating in different shading conditions, by using the equation below:

$$\Delta\theta_{\text{Loss}} = \frac{P_{\text{max}} - P_{Sha\_\text{max}}}{P_{\text{max}}}, \tag{6}$$

in which P_{max} and P_{Sha_max} are, respectively, the maximum power produced under normal (unshaded) and partial shading conditions.

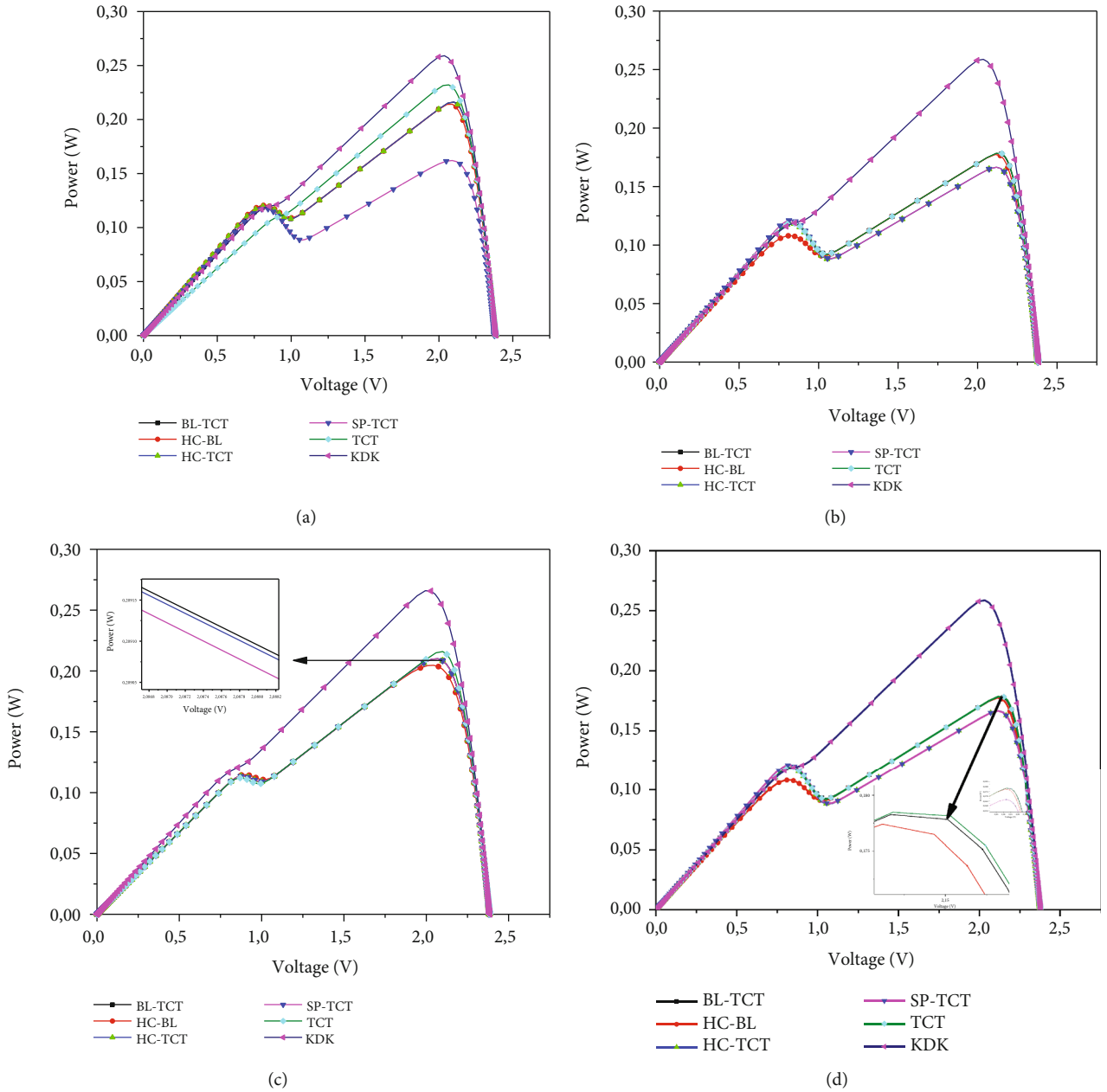

Figure 14: P-V characteristics of various PV module topologies operating in SS-pattern conditions: (a) SS-pattern A, (b) SS-pattern B, (c) SS-pattern C, and (d) SS-pattern D.

Figure 15 shows the relative power losses generated by TCT, BL-TCT, HC-BL, HC-TCT, SP-TCT, and KDK module topologies operating in homogeneous shading conditions. The results indicate how related the shading model and the power dissipation are. For DS-pattern condition shown in Figure 15 bar chart form, the KDK topology presents better performance compared to TCT, BL-TCT, HC-BL, HC-TCT, SP-TCT, and TCT. Most power dissipations are related to FS-pattern in which the shading has covered the entire PV module row. According to the VS-pattern, all topologies are found to be better in most of the shading models under homogeneous shading conditions. This implies that once the shading is distributed over the important part of the PV module area, the topologies do not constitute an alternative to power loss issues no matter the shading pattern. For the sectional shading shown in Figure 16, BL-TCT and KDK are considered as the topologies with the best efficiency in comparison to the others under CS-pattern condition. On the other hand, under CLS-pattern conditions, TCT and KDK are the most interesting. The results obtained demonstrate that the KDK topology gives the best efficiency, whereas the SP-TCT typology presents lower efficiency. This indicates that the junctions among the PV cells may have an effect over power generation. Figure 17 presents the simulated results of power losses for different topologies as a function of the defined scattered shading pattern. For these shading patterns, the power losses are quite drastic for the SP-TCT topology.

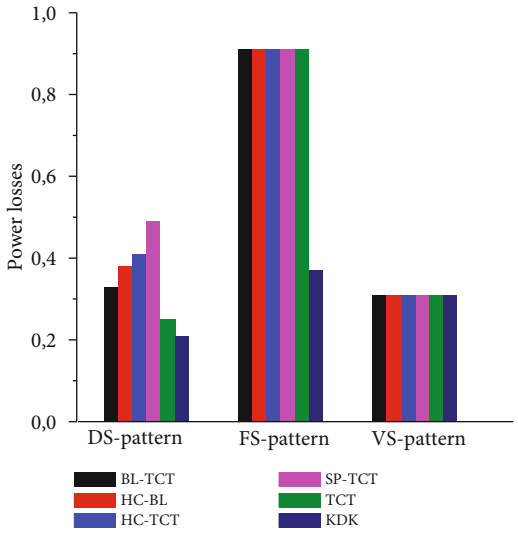

Figure 15: Power losses of the different topologies under homogeneous shading conditions.

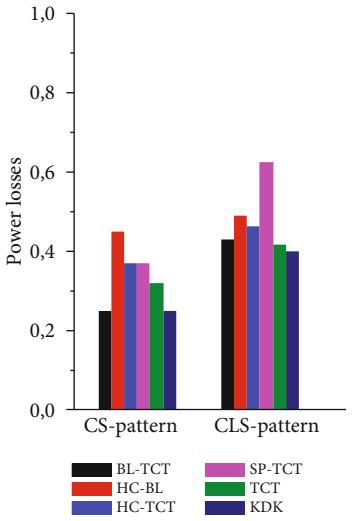

Figure 16: Power losses of the different topologies under sectional shading conditions.

Under SS-patterns A, B, and C, the KDK topology shows low power loss compared to the others. On the other hand, HC-TCT presents some efficiency comparable to that of KDK topology with low power losses under SS-pattern D condition.

The results obtained show a greater rate of degradation of the value of the maximum power compared to the initial values of:

(i) 36% in KDK topology and 91% in other topologies such as BL-TCT, HC-BL, HC-TCT, and SP-TCT operating under homogeneous shading condition, particularly in FS-pattern

(ii) 39% in KDK, 43% in BL-TCT, 49% in HC-BL, 46% in HC-TCT, 41% in TCT, and 62.6% in SP-TCT topologies under sectional shading condition, under the circumstances of CLS-pattern

(iii) 28% in KDK (SS-pattern A and C), 35% in BL-TCT (SS-pattern C), 39% in HC-BL (SS-pattern C), 42% in HC-TCT (SS-pattern C), 56% in SP-TCT (SS-pattern A), and 41% in TCT (SS-pattern A) topologies under scattered shading condition

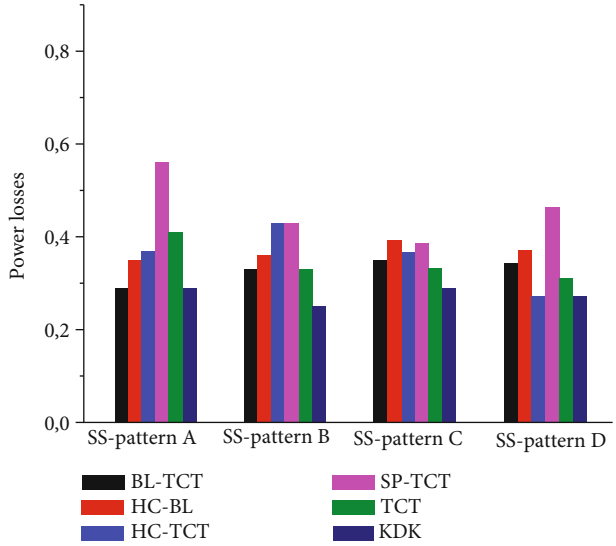

Figure 17: Power losses of the different topologies under scattered shading conditions.

5. Comparison with Existing Reconfigurations Topologies

In this section, the proposed KDK approach and existing reconfiguration topologies such as odd-even OE [25] and Latin square LS [26] are compared to evaluate their applicability under different partial shading conditions.

5.1. Factors Impacting the Effectiveness of PV Module Topologies. The main factors considered to test the effectiveness of these various topologies are global maximum power (GMP), mismatch power losses (MPL), fill factor (FF), and performance ratio (PR).

5.1.1. Mismatch Power Losses (MPL). MPL is defined as the difference in GMP under the standard test condition (STC) from partial shading conditions and can be formulated as

$$\text{MPL} = P_{\text{GMP}}(\text{STC}) - P_{\text{GMP}}(\text{PSc}), \tag{7}$$

where P_{GMP} (STC) and P_{GMP} (PSc) are the generated GMP at STC and PSc, respectively.

5.1.2. Fill Factor (FF). Fill factor can be defined as the ratio of GMP to the product of module's open-circuit voltage (V_{OC}) and short circuit current (I_{SC}) given by

$$\text{FF} = \frac{P_{\text{GMP}}}{V_{\text{OC}} \times I_{\text{SC}}} = \frac{V_{\text{GMP}} \times I_{\text{GMP}}}{V_{\text{OC}} \times I_{\text{SC}}}. \tag{8}$$

Table 2: Maximum power estimation for OE [25], LS [26], and KDK arrangement schemes of configuration under different partial shading conditions.

OE [25]			LS [26]			KDK		
Current in rows (A)	V (V)	P (W)	Current in rows (A)	V (V)	P (W)	Current in rows (A)	V (V)	P (W)
DS pattern								
$I_{row\,(1)} = 2.5\,I_m$	$3\,V_m$	$7.5\,V_m I_m$	$I_{row\,(1)} = 2.5\,I_m$	$3\,V_m$	$7.5\,V_m I_m$	$I_{row\,(1)} = 3\,I_m$	$3\,V_m$	$9\,V_m I_m$
$I_{row\,(2)} = 2\,I_m$	$3\,V_m$	$6\,V_m I_m$	$I_{row\,(2)} = 2\,I_m$	$3\,V_m$	$6\,V_m I_m$	$I_{row\,(2)} = 2\,I_m$	$3\,V_m$	$6\,V_m I_m$
$I_{row\,(3)} = 2\,I_m$	$3\,V_m$	$6\,V_m I_m$	$I_{row\,(3)} = 2\,I_m$	$3\,V_m$	$6\,V_m I_m$	$I_{row\,(3)} = 2\,I_m$	$3\,V_m$	$6\,V_m I_m$
$I_{row(4)} = 2.5\,I_m$	$3\,V_m$	$7.5\,V_m I_m$	$I_{row\,(4)} = 2.5\,I_m$	$3\,V_m$	$7.5\,V_m I_m$	$I_{row\,(4)} = 3\,I_m$	$3\,V_m$	$9\,V_m I_m$
FS pattern								
$I_{row\,(1)} = 1.4\,I_m$	$4\,V_m$	$5.6\,V_m I_m$	$I_{row\,(1)} = 1.4\,I_m$	$4\,V_m$	$5.6\,V_m I_m$	$I_{row(1)} = 4\,I_m$	$4\,V_m$	$16\,V_m I_m$
$I_{row\,(2)} = 0$	0	0	$I_{row\,(2)} = 0$	0	0	$I_{row\,(2)} = 0$	0	0
$I_{row\,(3)} = 0$	0	0	$I_{row\,(3)} = 0$	0	0	$I_{row\,(3)} = 0$	0	0
$I_{row(4)} = 1.4\,I_m$	$4\,V_m$	$5.6\,V_m I_m$	$I_{row(4)} = 1.4\,I_m$	$4\,V_m$	$5.6\,V_m I_m$	$I_{row(4)} = 4\,I_m$	$4\,V_m$	$16\,V_m I_m$
VS pattern								
$I_{row\,(1)} = 2\,I_m$	$4\,V_m$	$8\,V_m I_m$	$I_{row\,(1)} = 2\,I_m$	$4\,V_m$	$8\,V_m I_m$	$I_{row(1)} = 2\,I_m$	$4\,V_m$	$8\,V_m I_m$
$I_{row\,(2)} = 2\,I_m$	$2\,V_m$	$4\,V_m I_m$	$I_{row\,(2)} = 2\,I_m$	$2\,V_m$	$4\,V_m I_m$	$I_{row\,(2)} = 2\,I_m$	$2\,V_m$	$4\,V_m I_m$
$I_{row\,(3)} = 2\,I_m$	$2\,V_m$	$4\,V_m I_m$	$I_{row\,(3)} = 2\,I_m$	$2\,V_m$	$4\,V_m I_m$	$I_{row\,(3)} = 2\,I_m$	$2\,V_m$	$4\,V_m I_m$
$I_{row(4)} = 2\,I_m$	$4\,V_m$	$8\,V_m I_m$	$I_{row(4)} = 2\,I_m$	$4\,V_m$	$8\,V_m I_m$	$I_{row(4)} = 2\,I_m$	$4\,V_m$	$8\,V_m I_m$
CS pattern								
$I_{row\,(1)} = 2.5\,I_m$	$3\,V_m$	$7.5\,V_m I_m$	$I_{row\,(1)} = 2.5\,I_m$	$3\,V_m$	$7.5\,V_m I_m$	$I_{row(1)} = 2.5\,I_m$	$3\,V_m$	$7.5\,V_m I_m$
$I_{row(2)} = 3.2\,I_m$	$3\,V_m$	$9.6\,V_m I_m$	$I_{row(2)} = 3.2\,I_m$	$3\,V_m$	$9.6\,V_m I_m$	$I_{row(2)} = 3.2\,I_m$	$3\,V_m$	$9.6\,V_m I_m$
$I_{row\,(3)} = 4\,I_m$	$4\,V_m$	$16\,V_m I_m$	$I_{row\,(3)} = 4\,I_m$	$4\,V_m$	$16\,V_m I_m$	$I_{row\,(3)} = 4\,I_m$	$4\,V_m$	$16\,V_m I_m$
$I_{row(4)} = 4\,I_m$	$4\,V_m$	$16\,V_m I_m$	$I_{row(4)} = 4\,I_m$	$4\,V_m$	$16\,V_m I_m$	$I_{row(4)} = 4\,I_m$	$4\,V_m$	$16\,V_m I_m$
CLS pattern								
$I_{row\,(1)} = 4\,I_m$	$4\,V_m$	$16\,V_m \mathrm{I_m}$	$I_{row\,(1)} = 4\,I_m$	$4\,V_m$	$16\,V_m I_m$	$I_{row\,(1)} = 4\,I_m$	$4\,V_m$	$16\,V_m I_m$
$I_{row(2)} = 2.3\,I_m$	$2\,V_m$	$4.6\,V_m I_m$	$I_{row(2)} = 2.3\,I_m$	$2\,V_m$	$4.6\,V_m I_m$	$I_{row(2)} = 2.3\,I_m$	$3\,V_m$	$6.9\,V_m I_m$
$I_{row(3)} = 1.5\,I_m$	V_m	$1.5\,V_m I_m$	$I_{row(3)} = 1.5\,I_m$	$2\,V_m$	$3\,V_m I_m$	$I_{row(3)} = 2.5\,I_m$	$2\,V_m$	$5\,V_m I_m$
$I_{row(4)} = 4\,I_m$	$4\,V_m$	$16\,V_m I_m$	$I_{row(4)} = 4\,I_m$	$4\,V_m$	$16\,V_m I_m$	$I_{row(4)} = 4\,I_m$	$4\,V_m$	$16\,V_m I_m$
SS pattern A								
$I_{row\,(1)} = 2.3\,I_m$	$3\,V_m$	$6.9\,V_m I_m$	$I_{row\,(1)} = 3.1\,I_m$	$3\,V_m$	$9.3\,V_m I_m$	$I_{row(1)} = 3.2\,I_m$	$4\,V_m$	$12.8\,V_m I_m$
$I_{row(2)} = 3\,I_m$	$3\,V_m$	$9\,V_m I_m$	$I_{row(2)} = 3\,I_m$	$3\,V_m$	$9\,V_m I_m$	$I_{row(2)} = 4\,I_m$	$4\,V_m$	$16\,V_m I_m$
$I_{row(3)} = 3.5\,I_m$	$3\,V_m$	$10.5\,V_m I_m$	$I_{row(3)} = 3.5\,I_m$	$4\,V_m$	$14\,V_m I_m$	$I_{row(3)} = 4\,I_m$	$4\,V_m$	$16\,V_m I_m$
$I_{row(4)} = 3.9\,I_m$	$3\,V_m$	$15.6\,V_m I_m$	$I_{row(4)} = 3.9\,I_m$	$4\,V_m$	$15.6\,V_m I_m$	$I_{row(4)} = 3.9\,I_m$	$4\,V_m$	$15.6\,V_m I_m$
SS pattern B								
$I_{row\,(1)} = 4\,I_m$	$4\,V_m$	$16\,V_m I_m$	$I_{row\,(1)} = 4\,I_m$	$4\,V_m$	$16\,V_m I_m$	$I_{row\,(1)} = 4\,I_m$	$4\,V_m$	$16\,V_m I_m$
$I_{row(2)} = 4\,I_m$	$4\,V_m$	$16\,V_m I_m$	$I_{row(2)} = 4\,I_m$	$4\,V_m$	$16\,V_m I_m$	$I_{row(2)} = 4\,I_m$	$4\,V_m$	$16\,V_m I_m$
$I_{row(3)} = 3\,I_m$	$3\,V_m$	$9\,V_m I_m$	$I_{row(3)} = 3.1\,I_m$	$3\,V_m$	$9.3\,V_m I_m$	$I_{row(3)} = 3.9\,I_m$	$4\,V_m$	$15.6\,V_m I_m$
$I_{row(4)} = 1.7\,I_m$	$2\,V_m$	$3.4\,V_m I_m$	$I_{row(4)} = 2.4\,I_m$	$3\,V_m$	$7.2\,V_m I_m$	$I_{row(4)} = 2.4\,I_m$	$3\,V_m$	$7.2\,V_m I_m$
SS pattern C								
$I_{row\,(1)} = 2.1\,I_m$	$2\,V_m$	$4.2\,V_m I_m$	$I_{row\,(1)} = 2.1\,I_m$	$3\,V_m$	$6.3\,V_m I_m$	$I_{row\,(1)} = 2.1\,I_m$	$3\,V_m$	$6.3\,V_m I_m$
$I_{row(2)} = 3.1\,I_m$	$3\,V_m$	$9.3\,V_m I_m$	$I_{row(2)} = 3.2\,I_m$	$3\,V_m$	$9.6\,V_m I_m$	$I_{row(2)} = 3.9\,I_m$	$4\,V_m$	$15.6\,V_m I_m$
$I_{row(3)} = 3.5\,I_m$	$3\,V_m$	$10.5\,V_m I_m$	$I_{row(3)} = 3.5\,I_m$	$3\,V_m$	$10.5\,V_m I_m$	$I_{row(3)} = 3.5\,I_m$	$4\,V_m$	$14\,V_m I_m$

Table 2: Continued.

OE [25]			LS [26]			KDK		
Current in rows (A)	V (V)	P (W)	Current in rows (A)	V (V)	P (W)	Current in rows (A)	V (V)	P (W)
$I_{row(4)} = 4\,I_m$	$4\ V_m$	$16\ V_m\,I_m$	$I_{row(4)} = 4\,I_m$	$4\ V_m$	$16\ V_m\,I_m$	$I_{row(4)} = 4\,I_m$	$4\ V_m$	$16\ V_m\,I_m$
SS pattern D								
$I_{row\,(1)} = 2.1\,I_m$	$2\ V_m$	$4.2\ V_m\,I_m$	$I_{row\,(1)} = 3.1\,I_m$	$3\ V_m$	$4.2\ V_m\,I_m$	$I_{row\,(1)} = 9.3\,I_m$	$2\ V_m$	$9.3\ V_m\,I_m$
$I_{row(2)} = 4\,I_m$	$4\ V_m$	$16\ V_m\,I_m$	$I_{row(2)} = 4\,I_m$	$4\ V_m$	$9.3\ V_m\,I_m$	$I_{row(2)} = 16\,I_m$	$4\ V_m$	$16\ V_m\,I_m$
$I_{row(3)} = 3.1\,I_m$	$3\ V_m$	$9.3\ V_m\,I_m$	$I_{row(3)} = 3.1\,I_m$	$3\ V_m$	$10.5\ V_m\,I_m$	$I_{row(3)} = 9.3\,I_m$	$4\ V_m$	$13.6\ V_m\,I_m$
$I_{row(4)} = 3.5\,I_m$	$4\ V_m$	$14\ V_m\,I_m$	$I_{row(4)} = 3.5\,I_m$	$4\ V_m$	$16\ V_m\,I_m$	$I_{row(4)} = 14\,I_m$	$4\ V_m$	$15.6\ V_m\,I_m$

5.1.3. Performance Ratio (PR). PR is defined as the ratio of GMP under PSc and GMP at STC. It can be calculated using

$$\mathrm{PR} = \frac{P_{\mathrm{GMP}}(\mathrm{PSc})}{P_{\mathrm{GMP}}(\mathrm{STC})}. \tag{9}$$

5.2. Mathematical Analysis. For each partial shading conditions described in Section 3.2, the row currents are theoretically computed to locate the global maximum power. The current in each row is formulated as:

$$I_{\mathrm{row}}(i) = \sum_{k=1}^{4}\left(\frac{S_{ik}}{S_{\mathrm{STC}}} \times I_{ik}\right), \tag{10}$$

where I_{ik} is the current produced by the $(i,k)^{\mathrm{th}}$ cell, S_{ik} the irradiance of PV cell presented in i^{th} row and k^{th} column, and S_{STC} the irradiance of PV cell at STC ($S_{\mathrm{STC}} = 1000\,\mathrm{W/m^2}$).

Similarly, the voltage of the PV module can be determined using the following formula:

$$V_{\mathrm{mod}} = \sum_{i=1}^{m} V_{mi}, \tag{11}$$

where V_{mi} is the maximum voltage of the i^{th} row.

5.2.1. DS Pattern Condition. Under this shading pattern, the diagonally positioned cells in a PV module are subjected to distinct levels of irradiance. The shaded cells receive irradiance of $0\,\mathrm{W/m^2}$ and $500\,\mathrm{W/m^2}$ as shown in Figure 1(a). The remaining cells are shaded at $1000\,\mathrm{W/m^2}$.

(1) Current Generated from Kendoku PV Module. In the first and fourth rows, the generated row currents are determined as

$$\begin{aligned} I_{\mathrm{row}}(1) &= \left(\frac{0}{1000}\right) \times I_m + 3 \times \left(\frac{1000}{1000}\right) \times I_m \\ &= 3I_m = I_{\mathrm{row}}(4). \end{aligned} \tag{12}$$

In the second and third rows, the produced current is the same and is determined as:

$$\begin{aligned} I_{\mathrm{row}}(2) = I_{\mathrm{row}}(3) &= \left(\frac{0}{1000}\right) \times I_m + 2 \times \left(\frac{500}{1000}\right) \\ &\times I_m + \left(\frac{1000}{1000}\right) \times I_m = 2 \times I_m. \end{aligned} \tag{13}$$

(2) Current Generated from OE Topology. From the OE topology, the currents produced in the first and fourth rows are determined as:

$$\begin{aligned} I_{\mathrm{row}}(1) = I_{\mathrm{row}}(4) &= \left(\frac{0}{1000}\right) \times I_m + \left(\frac{500}{1000}\right) \\ &\times I_m + 2 \times \left(\frac{1000}{1000}\right) \times I_m = 2.5I_m. \end{aligned} \tag{14}$$

Similarly, the current generated for the remaining rows are calculated as:

$$\begin{aligned} I_{\mathrm{row}}(2) = I_{\mathrm{row}}(3) &= \left(\frac{0}{1000}\right) \times I_m + 2 \times \left(\frac{500}{1000}\right) \\ &\times I_m + \left(\frac{1000}{1000}\right) \times I_m = 2 \times I_m. \end{aligned} \tag{15}$$

(3) Current Generated Form LS Topology. For four rows of cells in the LS configuration, the current in each row is determined separately as:

$$\begin{aligned} I_{\mathrm{row}}(1) = I_{\mathrm{row}}(4) &= \left(\frac{0}{1000}\right) \times I_m + \left(\frac{500}{1000}\right) \\ &\times I_m + 2 \times \left(\frac{1000}{1000}\right) \times I_m = 2.5I_m, \end{aligned} \tag{16}$$

$$\begin{aligned} I_{\mathrm{row}}(2) = I_{\mathrm{row}}(3) &= \left(\frac{0}{1000}\right) \times I_m + 2 \times \left(\frac{500}{1000}\right) \\ &\times I_m + \left(\frac{1000}{1000}\right) \times I_m = 2 \times I_m. \end{aligned} \tag{17}$$

The approximate row current, voltage, and power for OE, LS, and KDK configurations under DS pattern

Table 3: Performance factors such as GMP, MPL, FF, and PR of OE [25], LS [26], and KDK arrangement schemes of configuration under different partial shading conditions.

Configurations	GMP Ia (A)	GMP Va (V)	Pa (W)	MPL (%)	FF (%)	PR (%)	Best configuration
				DS pattern			
OE [25]	0.112	1.503	0.168	54.35	53.33	45.60	
LS [26]	0.112	1.503	0.168	54.35	53.33	45.60	KDK
KDK	0.133	1.503	0.199	46.00	63.20	54.08	
				FS pattern			
OE [25]	0.0625	2.004	0.125	66.03	39.70	33.90	
LS [26]	0.112	2.004	0.224	39.13	71.10	60.90	KDK
KDK	0.143	1.890	0.275	25.3	87.30	74.70	
				VS pattern			
OE [25]	0.089	2.004	0.178	51.60	56.50	48.40	
LS [26]	0.089	2.004	0.178	51.60	56.50	48.40	OE/LS/KDK
KDK	0.089	2.004	0.178	51.60	56.50	48.40	
				CS pattern			
OE [25]	0.143	1.890	0.275	25.30	87.30	74.70	
LS [26]	0.143	1.890	0.275	25.30	87.30	74.70	OE/LS/KDK
KDK	0.143	1.890	0.275	25.30	87.30	74.70	
				CLS pattern			
OE [25]	0.067	0.501	0.033	91.03	10.50	8.90	
LS [26]	0.067	1.002	0.067	82.80	21.30	18.20	KDK
KDK	0.112	1.002	0.112	69.60	35.50	35.50	
				SS pattern A			
OE [25]	0.143	1.503	0.215	41.60	68.20	58.40	
LS [26]	0.143	1.890	0.275	25.30	87.30	74.70	LS/KDK
KDK	0.143	1.890	0.275	25.30	87.30	74.70	
				SS pattern B			
OE [25]	0.134	1.503	0.201	45.00	63.80	54.60	
LS [26]	0.138	1.503	0.207	44.00	65.70	56.20	KDK
KDK	0.143	1.890	0.275	25.30	87.30	74.7	
				SS pattern C			
OE [25]	0.138	1.503	0.207	44.00	65.70	56.20	
LS [26]	0.142	1.503	0.213	42.00	67.60	57.80	KDK
KDK	0.143	1.890	0.275	25.30	87.30	74.7	
				SS pattern D			
OE [25]	0.138	1.503	0.207	44.00	65.70	56.20	
LS [26]	0.138	1.503	0.207	44.00	65.70	56.20	KDK
KDK	0.143	1.890	0.275	25.30	87.30	74.7	

condition are listed in Table 2. The improved effectiveness is carried out after the novel arrangement of PV cells according to the KDK approach. The calculated power is found higher or equal. Indeed, in the KDK configuration, the repositioning of PV cells disperses the PSc effects over the PV module, which results in improved maximum power.

5.2.2. FS Pattern Condition. As illustrated in Figure 1(b), the PV cells in rows 2 and 3 are completely shaded. The calculated row current, voltage, and power of OE, LS, and KDK configurations under this shading pattern are tabulated in Table 2. It is obvious that after the rearrangement of PV cells according to the KDK approach, the KDK topology increased power generation compared to OE and LS configurations.

5.2.3. VS Pattern Condition. Under this shading pattern, the PV cells in columns 2 and 3 are completely shaded, as shown in Figure 1(c). Table 2 presents the calculated current, voltage, and power of the OE, LS, and KDK configurations. In

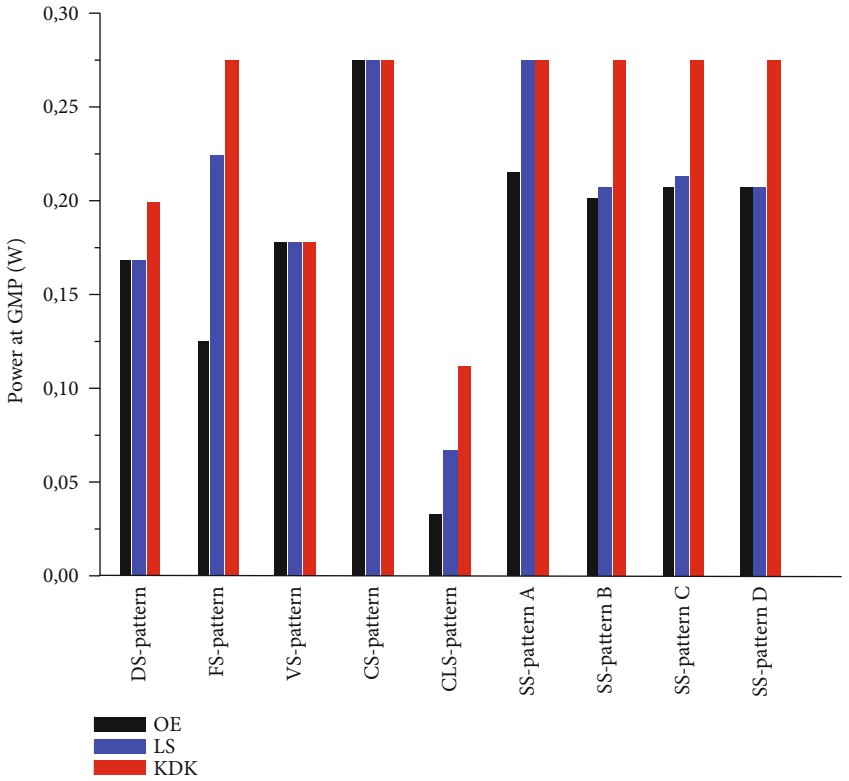

Figure 18: Effects of partial shading patterns on power (at MPP).

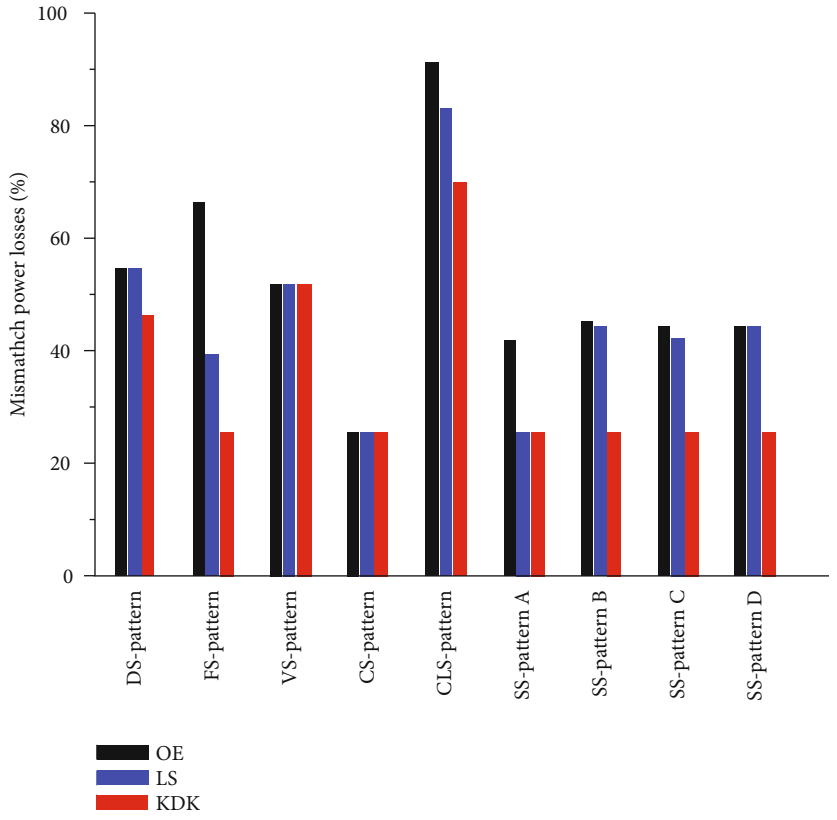

Figure 19: Effects of partial shading patterns on mismatch power losses.

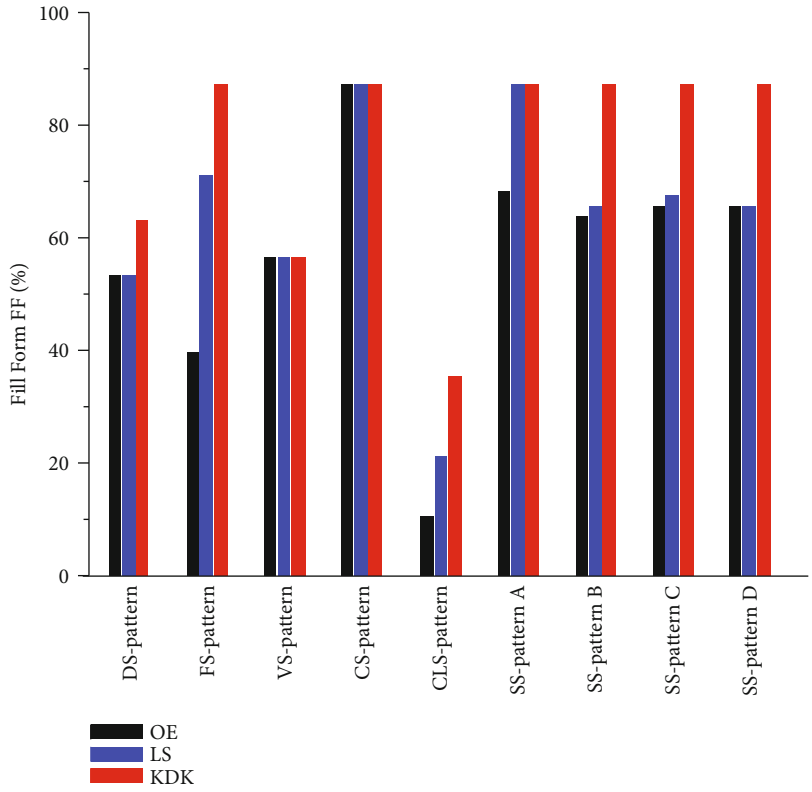

Figure 20: Effects of partial shading patterns on fill factor.

Table 4: Parameters of PV cell (1000 W/m^2, 25°C).

Cell parameters	Values
V_{OC}(mV)	630
I_{SC}(mA/cm^2)	42.4
V_{mpp}(mV)	501
I_{mpp}(mA/cm^2)	37.2
P_{mpp}(mW/cm^2)	18.6
FF(%)	>70

this shading pattern, the calculated power is found to be the same value in all of the configurations considered.

5.2.4. CS Pattern Condition. As shown in Figure 1(d), the three PV cells positioned in the left corner are subjected to different irradiance levels. Shaded PV cells receive 0 W/m^2, 200 W/m^2, and 500 W/m^2. The rest of the PV cells receive 1000 W/m^2. Table 2 shows the calculated current, voltage, and power of OE, LS, and KDK configurations. The results shows that OE, LS, and KDK generated maximum power by dispersing more shades over the PV module.

5.2.5. CLS Pattern Condition. As seen in Figure 1(e), the center-positioned PV cells are subjected to different irradiance levels. The shaded PV cells receive 0 W/m^2, 100 W/m^2, 200 W/m^2, and 500 W/m^2. The remaining shaded PV cells 1000 W/m^2 irradiance. Table 2 shows the calculated current, voltage, and power of OE, LS, and KDK configurations. The results of the KDK configuration present improved performance for this shading pattern over the OE and LS configurations.

5.2.6. SS Pattern A Condition. As presented in Figure 1(f), the SS-positioned PV cells are submitted to different irradiance levels. The shaded PV cells receive 0 W/m^2, 100 W/m^2, 200 W/m^2, 500 W/m^2, and 900 W/m^2. The remaining cells receive irradiance of 1000 W/m^2. Table 2 presents the calculated row current, voltage, and power of the OE, LS, and KDK configurations. According to the obtained results, the KDK configuration shows improved performance when compared to OE and LS configurations.

5.2.7. SS Pattern B Condition. As described in Figure 1(g), the positioned PV cells are subjugated to different irradiance levels. The shaded PV cells receive irradiance of 0 W/m^2, 100 W/m^2, 200 W/m^2, and 900 W/m^2. The rest of the PV cells receive 1000 W/m^2 irradiance. The calculated row current, voltage, and power for OE, LS, and KDK configurations are shown in Table 2. From this table, it is clearly noted that the KDK and LS configurations show improved performance as compared to OE PV cell arrangement.

5.2.8. SS Pattern C Condition. As shown in Figure 1(h), the PV cells positioned in columns 1 and 2 are subjected to different levels of irradiance. The shaded PV cells receive 0 W/m^2, 100 W/m^2, 200 W/m^2, 500 W/m^2, and 900 W/m^2 irradiances. The rest of the PV cells receive 1000 W/m^2. Table 2

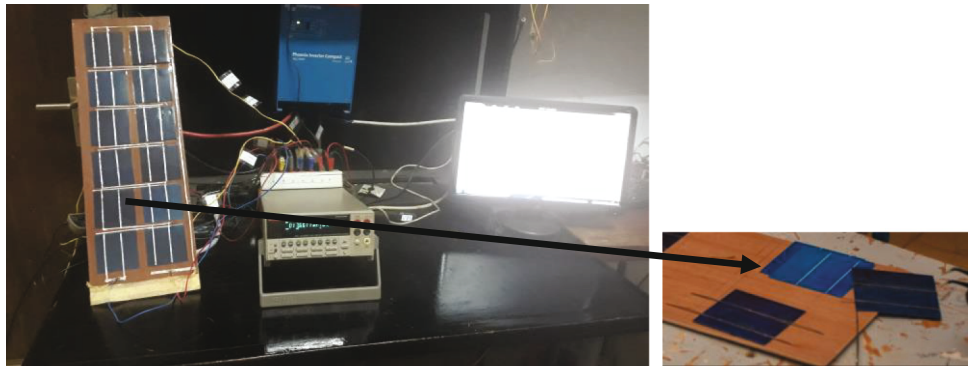

Figure 21: Experimental setup.

Table 5: Experimental results.

Shading pattern	Power obtained (mW)			
	Ideal power	OE [25]	LS [26]	KDK
DS-pattern		101.3	102.1	119.4
FS-pattern		76.06	134.7	164.85
VS-pattern		105.4	105.3	105.5
CS-pattern		162.85	162.85	162.85
CLS-pattern	218	20.56	38.5	67.28
SS-pattern A		128.31	163.85	163.85
SS-pattern B		120.9	122.08	162.85
SS-pattern C		122.08	126.5	163.85
SS-pattern D		122.08	122.08	163.85

shows the approximate row current, voltage, and power for OE, LS, and KDK configurations under this shading condition. The obtained results of the KDK topology show improved performance compared to the arrangement of OE and LS PV cells.

5.2.9. SS Pattern D Condition. As illustrated in Figure 1(i), the positioned PV cells are subdued to different irradiance levels. The shaded PV cells receive 0 W/m^2, 100 W/m^2, 200 W/m^2, 500 W/m^2, and 900 W/m^2 irradiances. The rest of the PV cells receive 1000 W/m^2. Table 2 shows the calculated row current, voltage, and power for OE, LS, and KDK PV cell arrangements. From this table, improved effectiveness is obtained after the novel arrangement of PV cells, according to the KDK approach compared to OE and LS configuration.

5.3. GMP, MPL, FF, and PR Comparison. In this section, for a better understanding, performance factors of OE, LS, and KDK are tabulated in Table 3 under different partial shading conditions.

After implementing the different approaches named OE, LS, and KDK to reconfigure the PV cells and distribute shades on its area to extract maximum power, the obtained results of each in terms of GMP are analyzed and compared. Figure 18 shows the effects of shading on power generation.

The results show that the KDK approach generates the best GMP for most of the considered shading patterns compared to OE and Ls methods. Analysis of results by MPL, FF, and PR factors under different shading patterns is shown in Figures 19 and 20.

Based on the analysis performed in Figure 20, it can be noted that the KDK method is able to generate the best results in performance analysis via fill form (FF) factor compared to OE and LS methods. Evaluations also show that the KDK approach has the lowest of MPL compared to the other.

5.4. Experimental Analysis. An experimental setup has been carried out by using the PV cell configured with the proposed KenDoKu technique and the OE and the LS techniques. The electrical parameters of the PV cells under consideration are tabulated in Table 4. We have considered all shading patterns defined in Section 3.2. Figure 21 displays the experimental setup which consists in a Keithley 2701 multimeters, a simulator, and an arc lamp source. The data were recorded with a computer. To provide nonuniform insolation to the PV module, light-emitting diode lamps are used over each PV cell as independent source. The illumination of each lamp is controlled by using potentiometers connected across a light-emitting diode lamp. This allowed us to create partial shading conditions for the PV module.

Table 5 summarizes the experimental powers obtained by the proposed KDK reconfiguration and OE and LS reconfigurations under different shading conditions.

For the DS condition, the proposed KDK configuration has increased the maximum power by 8% compared to OE and LS techniques. For FS condition, the KDK configuration has raised the maximum power by 40.7% and 13.8% compared to OE and LS configurations, respectively. For VS and CS conditions, all the three KDK, OE, and LS configurations have generated the same maximum power of 105 mW (VS pattern) and 162.85 mW (CS pattern). For CLS condition, the KDK configuration has increased the maximum by 21.43% and 13.2% compared to OE and LS configurations, respectively. For the SS pattern A condition, the KDK and LS configurations have generated the best maximum power (163.85 mW) and raised the maximum power by 16.30% compared to the OE configuration. For the remaining partial shading conditions, the KDK configuration has generated the best maximum power output as compared to other OE and LS configurations. Overall, the

experimental data show that the proposed KDK technique resulted in a significant improvement in the maximum power of the PV module. Indeed, the KDK technique has reduced the shading loss by scatting more shades in all rows of the PV module. Besides, the KDK technique reorients the physical position of the PV cell within the PV module without altering the electrical interconnection. As the KDK technique does not use neither a complex algorithm nor a sensor and switching circuit, it can also be economical compared to other OE and LS configurations.

6. Conclusion

In this research paper, the effectiveness of TCT, BL-TCT, HC-BL, HC-TCT, SP-TCT, OE, and LS configurations is evaluated, analyzed, and compared with the proposed KDK arrangement scheme of configuration under defined partial shading conditions. The proposed KDK technique redistributed shading effects over the PV module without any change in the electrical connections of the PV cells. The effectiveness of the KDK approach is evaluated in terms of P-V curve characteristics, GMP, ML (%), FF (%), and PR (%). The simulation model is developed using the bishop model and is implemented in LTSpice software. The simulated results showed that the proposed KDK configuration scheme exhibited better performance to generate maximum power output under the considered partial shading conditions. In most of the cases, the GMP of the KDK configuration is found to be superior as compared to the existing OE and LS configurations. In short, the proposed KDK scheme of configuration has more efficiency as compared to the TCT, BL-TCT, HC-BL, HC-TCT, SP-TCT, OE, and LS schemes of interconnection, with an increasing maximum performance. In addition, the proposed approach reduced the maximum power losses (ML) and improved the fill factor (FF) with respect to the OE and LS configurations in most cases. Moreover, experimental verification is also carried out. The results obtained showed that the KDK configuration scheme outperforms other analyzed PV cell/module arrangement pattern of interconnection in terms of power increasing.

Data Availability

Data are available on request.

Conflicts of Interest

The authors declare that there is no conflict of interests regarding the publication of this paper.

Acknowledgments

The authors wish to express their gratitude to the Laboratory of Materials and Environment (LA.M.E), Burkina Faso, and the Group of electrical engineering, Paris (GeePs), who permit to realize the experimental setup.

References

[1] G. Sai Krishna and T. Moger, "Improved SuDoKu reconfiguration technique for total-cross-tied PV array to enhance maximum power under partial shading conditions," *Renewable and Sustainable Energy Reviews*, vol. 109, pp. 333–348, 2019.

[2] M. Premkumar, U. Subramaniam, T. S. Babu, R. M. Elavarasan, and L. Mihet-Popa, "Evaluation of mathematical model to characterize the performance of conventional and hybrid PV array topologies under static and dynamic shading patterns," *Energies*, vol. 13, no. 12, p. 3216, 2020.

[3] P. K. Bonthagorla and S. Mikkili, "Performance analysis of PV array configurations (SP, BL, HC and TT) to enhance maximum power under non-uniform shading conditions," in *Engineering Reports*, John Wiley & Sons, Ltd., 2020.

[4] S. R. Pendem and S. Mikkili, "Modelling and performance assessment of PV array topologies under partial shading conditions to mitigate the mismatching power losses," *Solar Energy*, vol. 160, pp. 303–321, 2018.

[5] H. S. Sahu and S. K. Nayak, "Power enhancement of partially shaded PV array by using a novel approach for shade dispersion," in *2014 IEEE Innovative Smart Grid Technologies-Asia (ISGT ASIA)*, pp. 498–503, Kuala Lumpur, Malaysia, 2014.

[6] P. Manoharan, U. Subramaniam, T. S. Babu et al., "Improved perturb and observation maximum power point tracking technique for solar photovoltaic power generation systems," *IEEE Systems Journal*, vol. 15, no. 2, pp. 3024–3035, 2021.

[7] L. L. Jiang, D. L. Maskell, and J. C. Patra, "A novel ant colony optimization-based maximum power point tracking for photovoltaic systems under partially shaded conditions," *Energy and Buildings*, vol. 58, pp. 227–236, 2013.

[8] M. Z. S. El-Dein, M. Kazerani, and M. M. A. Salama, "Novel configurations for photovoltaic farms to reduce partial shading losses," in *IEEE Power and Energy Society General Meeting*, Detroit, MI, USA, 2011.

[9] K.-H. Chao, P.-L. Lai, and B.-J. Liao, "The optimal configuration of photovoltaic module arrays based on adaptive switching controls," *Energy Conversion and Management*, vol. 100, pp. 157–167, 2015.

[10] K. Chen, D. Chen, Y. Zhu, and H. Shen, "Study of crystalline silicon solar cells with integrated bypass diodes," *Science China Technological Sciences*, vol. 55, no. 3, pp. 594–599, 2012.

[11] A. Bernardini, A. Sarti, P. Maffezzoni, and L. Daniel, "Wave digital-based variability analysis of electrical mismatch in photovoltaic arrays," in *2018 IEEE International Symposium on Circuits and Systems (ISCAS)*, Florence, Italy, 2018.

[12] F. Belhachat and C. Larbes, "Modeling, analysis and comparison of solar photovoltaic array configurations under partial shading conditions," *Solar Energy*, vol. 120, pp. 399–418, 2015.

[13] G. Sagar, D. Pathak, P. Gaur, and V. Jain, "A Su Do Ku puzzle based shade dispersion for maximum power enhancement of partially shaded hybrid bridge-link-total-cross-tied PV array," *Solar Energy*, vol. 204, pp. 161–180, 2020.

[14] S. Mohammadnejad, A. Khalafi, and S. M. Ahmadi, "Mathematical analysis of total-cross-tied photovoltaic array under partial shading condition and its comparison with other configurations," *Solar Energy*, vol. 133, pp. 501–511, 2016.

[15] L. F. L. Villa, D. Picault, B. Raison, S. Bacha, and A. Labonne, "Maximizing the power output of partially shaded photovoltaic plants through optimization of the interconnections among its modules," *IEEE Journal of Photovoltaics*, vol. 2, no. 2, pp. 154–163, 2012.

[16] D. La Manna, E. R. Sanseverino, V. Di Dio, and P. Romano, "Reconfigurable electrical interconnection strategies for photovoltaic arrays: a review," *Renewable and Sustainable Energy Reviews*, vol. 33, pp. 412–426, 2014.

[17] G. Sai Krishna and T. Moger, "Reconfiguration strategies for reducing partial shading effects in photovoltaic arrays: state of the art," *Solar Energy*, vol. 182, pp. 429–452, 2019.

[18] M. Z. Shams El-Dein, M. Kazerani, and M. M. A. Salama, "Optimal photovoltaic array reconfiguration to reduce partial shading losses," *IEEE Transactions on Sustainable Energy*, vol. 4, no. 1, pp. 145–153, 2013.

[19] G. S. Krishna and T. Moger, "Enhancement of maximum power output through reconfiguration techniques under non-uniform irradiance conditions," *Energy*, vol. 187, article 115917, 2019.

[20] K. Ş. Parlak, "PV array reconfiguration method under partial shading conditions," *International Journal of Electrical Power & Energy Systems*, vol. 63, pp. 713–721, 2014.

[21] A. S. Yadav, R. K. Pachauri, Y. K. Chauhan, S. Choudhury, and R. Singh, "Performance enhancement of partially shaded PV array using novel shade dispersion effect on magic-square puzzle configuration," *Solar Energy*, vol. 144, pp. 780–797, 2017.

[22] H. S. Sahu, S. K. Nayak, and S. Mishra, "Maximizing the power generation of a partially shaded PV array," *IEEE Journal of Emerging and Selected Topics in Power Electronics*, vol. 4, no. 2, pp. 626–637, 2016.

[23] M. Horoufiany and R. Ghandehari, "Optimization of the Sudoku based reconfiguration technique for PV arrays power enhancement under mutual shading conditions," *Solar Energy*, vol. 159, pp. 1037–1046, 2018.

[24] S. Vijayalekshmy, G. R. Bindu, and S. Rama Iyer, "A novel Zig-Zag scheme for power enhancement of partially shaded solar arrays," *Solar Energy*, vol. 135, pp. 92–102, 2016.

[25] I. Nasiruddin, S. Khatoon, M. F. Jalil, and R. C. Bansal, "Shade diffusion of partial shaded PV array by using odd-even structure," *Solar Energy*, vol. 181, pp. 519–529, 2019.

[26] R. Pachauri, A. S. Yadav, Y. K. Chauhan, A. Sharma, and V. Kumar, "Shade dispersion-based photovoltaic array configurations for performance enhancement under partial shading conditions," *International Transactions on Electrical Energy Systems*, vol. 28, no. 7, article e2556, 2018.

[27] F. Belhachat and C. Larbes, "PV array reconfiguration techniques for maximum power optimization under partial shading conditions: a review," *Solar Energy*, vol. 230, pp. 558–582, 2021.

[28] J. W. Bishop, "Computer simulation of the effects of electrical mismatches in photovoltaic cell interconnection circuits," *Solar Cells*, vol. 25, no. 1, pp. 73–89, 1988.

[29] Y.-J. Wang and P.-C. Hsu, "An investigation on partial shading of PV modules with different connection configurations of PV cells," *Energy*, vol. 36, no. 5, pp. 3069–3078, 2011.

[30] D. Bonkoungou, T. Guingane, E. Korsaga et al., "Measurements and analysis of the dark I-V-T characteristics of a photovoltaic cell: KX0B22-12X1F," in *2020 8th International Conference on Smart Grid (icSmartGrid)*, pp. 157–162, Paris, France, 2020.

[31] D. Bonkoungou, T. Guingane, E. Korsaga et al., "Parameters degradation analysis of a silicon solar cell in dark/light condition using measured I-V data," *Advances in Science, Technology and Engineering Systems Journal*, vol. 6, no. 1, pp. 1151–1156, 2021.